Atmos. Chem. Phys., 15, 319–334, 2015
www.atmos-chem-phys.net/15/319/2015/
doi:10.5194/acp-15-319-2015

Atmospheric Chemistry and Physics
Open Access

Estimation of PM_{10} concentrations over Seoul using multiple empirical models with AERONET and MODIS data collected during the DRAGON-Asia campaign

S. Seo[1,*], J. Kim[1], H. Lee[1,2], U. Jeong[1], W. Kim[1], B. N. Holben[3], S.-W. Kim[4], C. H. Song[5], and J. H. Lim[6]

[1]Institute of Earth, Astronomy, and Atmosphere, Brain Korea 21 Plus Program, Department of Atmospheric Sciences, Yonsei University, Seoul, South Korea
[2]Department of Spatial Information Engineering, Pukyong National University, Busan, South Korea
[3]NASA Goddard Space Flight Center, Greenbelt, MD, USA
[4]School of Earth and Environmental Sciences, Seoul National University, Seoul, South Korea
[5]School of Environmental Science and Engineering, GIST, Gwangju, South Korea
[6]Global Environment Research Division, National Institute of Environmental Research, Incheon, South Korea
[*]now at: Korea Polar Research Institute, Incheon, South Korea

Correspondence to: J. Kim (jkim2@yonsei.ac.kr)

Received: 30 June 2014 – Published in Atmos. Chem. Phys. Discuss.: 25 August 2014
Revised: 16 November 2014 – Accepted: 6 December 2014 – Published: 13 January 2015

Abstract. The performance of various empirical linear models to estimate the concentrations of surface-level particulate matter with a diameter less than 10 µm (PM_{10}) was evaluated using Aerosol Robotic Network (AERONET) sun photometer and Moderate-Resolution Imaging Spectroradiometer (MODIS) data collected in Seoul during the Distributed Regional Aerosol Gridded Observation Network (DRAGON)-Asia campaign from March to May 2012. An observed relationship between the PM_{10} concentration and the aerosol optical depth (AOD) was accounted for by several parameters in the empirical models, including boundary layer height (BLH), relative humidity (RH), and effective radius of the aerosol size distribution (R_{eff}), which was used here for the first time in empirical modeling. Among various empirical models, the model which incorporates both BLH and R_{eff} showed the highest correlation, which indicates the strong influence of BLH and R_{eff} on the PM_{10} estimations. Meanwhile, the effect of RH on the relationship between AOD and PM_{10} appeared to be negligible during the campaign period (spring), when RH is generally low in northeast Asia. A large spatial dependency of the empirical model performance was found by categorizing the locations of the collected data into three different site types, which varied in terms of the distances between instruments and source locations. When both AERONET and MODIS data sets were used in the PM_{10} estimation, the highest correlations between measured and estimated values ($R = 0.76$ and 0.76 using AERONET and MODIS data, respectively) were found for the residential area (RA) site type, while the poorest correlations ($R = 0.61$ and 0.68 using AERONET and MODIS data, respectively) were found for the near-source (NS) site type. Significant seasonal variations of empirical model performances for PM_{10} estimation were found using the data collected at Yonsei University (one of the DRAGON campaign sites) over a period of 17 months including the DRAGON campaign period. The best correlation between measured and estimated PM_{10} concentrations ($R = 0.81$) was found in winter, due to the presence of a stagnant air mass and low BLH conditions, which may have resulted in relatively homogeneous aerosol properties within the BLH. On the other hand, the poorest correlation between measured and estimated PM_{10} concentrations ($R = 0.54$) was found in spring, due to the influence of the long-range transport of dust to both within and above the BLH.

Published by Copernicus Publications on behalf of the European Geosciences Union.

Table 1. Previous studies associated with the estimation of PM concentrations using AOD.

Method	Study area	Data		R	Reference
		AOD	PM_x		
MT1[a]	Northern Italy	Daily sun photometer	Daily PM_{10}	0.82	Chu et al. (2003)
MT1	Alabama	MODIS (10 km)	$PM_{2.5}$	0.70	Wang and Christopher (2003)
MT1	Southeastern US	MODIS (10 km)	$PM_{2.5}$	0.40	Engel-Cox et al. (2004)
			Daily $PM_{2.5}$	0.43	
MT1	US	MODIS	$PM_{2.5}$	0.52	Gupta and Christopher (2008)
			Daily $PM_{2.5}$	0.62	
MT1	Cabauw	Sun photometer	$PM_{2.5}$	0.75	Schaap et al. (2009)
		MODIS (10 km)		0.72	
MT2[b]	Europe	MODIS (10 km)	$PM_{2.5}$	0.60	Koelemeijer et al. (2006)
			PM_{10}	0.50	
MT2	Alpine region	SEVIRI	Daily PM_{10}	0.70	Emili et al. (2010)
		MODIS		0.60	
MT2	Beijing	MODIS (1 km)	$PM_{2.5}$	0.68	Wang et al. (2010)
			PM_{10}	0.68	
MT3[c]	Eastern US	MISR	Daily $PM_{2.5}$	0.69	Liu et al. (2005)
MT3	St. Louis	MISR	Daily $PM_{2.5}$	0.79	Liu et al. (2007)
		MODIS		0.71	
MT3	Lille	Sun photometer	PM_{10}	0.87	Pelletier et al. (2007)
MT4[d]	US	MISR	Yearly $PM_{2.5}$	0.78	Liu et al. (2004)
MT4	East Asia	MODIS	Seasonal PM_{10}	0.28–0.54	Choi et al. (2009)

[a] MT1 uses the empirical linear relationship between AOD and PM_x ($PM_x = a\,AOD + b$).
[b] MT2 uses the empirical linear relationship between corrected AOD (vertical distribution, RH) and PM_x.
[c] MT3 uses the poly-parameter model.
[d] MT4 uses the 3-D atmospheric chemistry model.

1 Introduction

Atmospheric aerosols are known to play an important role in not only air quality but also climate change (Kaufman et al., 2002; WHO, 2005; IPCC, 2013). In terms of air quality, surface-level aerosol concentrations have been found to be strongly associated with impaired visibility (Baumer et al., 2008) and adverse effects on human health, such as respiratory and cardiovascular diseases (Pope et al., 2002; Kappos et al., 2004; Brook et al., 2010; Brauer et al., 2012). Therefore, several ground-based aerosol monitoring networks, such as the Interagency Monitoring of Protected Visual Environments (IMPROVE; http://vista.cira.colostate.edu/improve/) and the EPA's State and Local Air Monitoring Stations (SLAMS; http://www.epa.gov/ttn/amtic/slams.html), have been installed and operated to further understand the spatial and temporal variability of the chemical and physical characteristics of aerosols (Wang and Christopher, 2003).

However, due to the spatial limitations of in situ measurements, the coordination of dense networks of multiple sites is required to monitor spatial variations in surface air quality in certain areas. To overcome the spatial limitations of such in situ measurements, additional efforts have been made to estimate surface air quality from satellite measurements. Table 1 summarizes the implementation of several different approaches that have been used to derive surface particulate matter (PM) concentrations using aerosol optical depth (AOD) measurements obtained from sun photometer and satellite instruments. An empirical linear model using only AOD as a predictor for PM estimation showed correlation coefficients between measured and predicted $PM_{2.5}$ of 0.2–0.75 (Chu et al., 2003; Wang and Christopher, 2003; Engel-Cox et al., 2004; Gupta and Christopher, 2008; Schaap et al., 2009). When the additional effects of boundary layer height (BLH) and relative humidity (RH) were incorporated into the empirical linear model (Engel-Cox et al., 2006; Koelemeijer et al., 2006; Emili et al., 2010; Wang et al., 2010), correlations between measured and predicted $PM_{2.5}$ were further improved when compared with correlations obtained from linear models using only AOD. A multiple linear regression model between measured and predicted $PM_{2.5}$ concentrations in urban areas yielded a correlation of 0.71 (Liu et al., 2007). Spatial distributions of $PM_{2.5}$ can also be estimated by applying the ratio of AOD to $PM_{2.5}$, as calculated from chemical transport models (CTMs), such as the Goddard Earth Observing System-Chemistry (GEOS-CHEM) transport model and the Community Multiscale Air Quality (CMAQ) model (Liu et al., 2004; Choi et al., 2009; van Donkelaar et al., 2010). These previous studies have demonstrated the strong possibility of deriving surface PM concentrations from AOD data.

However, if we are to further improve and validate PM estimates, additional physical parameters should be considered as inputs into the empirical models, so as to obtain accurate estimates of PM concentrations from AOD data. Additionally, the effects of various environmental characteristics on the relationship between PM and AOD, as well as spatial and temporal variations in this relationship, need to be investigated, especially in complex urban regions which include aerosol particles generated from various industrial and residential sources. Despite the need to monitor the rapidly changing PM concentrations in megacities with large populations and many sources of pollution, only a small number of studies have been conducted, especially in Asia, and the numbers of ground-based PM monitoring stations in these studies have been limited (Kumar et al., 2007; Guo et al., 2009). In addition to limitations based on sample size, obtaining accurate estimates of PM from AOD data has proved difficult in Asia on account of the complexity of the aerosol compositions derived from both natural and anthropogenic sources, particularly during the spring (Kim et al., 2007; Song et al., 2009; Lee et al., 2010).

In an effort to address these problems, the present study uses aerosol measurements collected during the Distributed Regional Aerosol Gridded Observation Network (DRAGON)-Asia 2012 campaign, which is just one of the DRAGON campaigns that has been conducted globally (http://aeronet.gsfc.nasa.gov/new_web/DRAGON-Asia_2012_Japan_South_Korea.html). The intensive DRAGON campaigns have provided valuable data sets, with well-coordinated measurements made in areas where aerosol concentrations are highly variable in space and time, and dependent on sources and other factors. The DRAGON campaigns have been conducted in urban and industrial areas, including Washington D.C., the San Joaquin Valley of California, and the Houston metropolitan region of Texas. By using the campaign data sets obtained from the dense coverage of both column and surface-level aerosol measurements, assessments of surface-level PM concentrations based on remote sensing observations can be substantially improved, especially in spring.

The purpose of this study is to investigate the relationship between AOD and PM concentrations in Seoul, one of the largest megacities in northeast Asia, using the DRAGON-Asia campaign data set. The detailed objectives of this study are (1) to estimate PM_{10} concentrations using AOD data from both ground- and satellite-based measurements in a megacity, with additional consideration of the various parameters within the empirical models, and to thereby evaluate derived PM concentrations; (2) to identify the spatial variability of the empirical model performance at different types of measurement site; and (3) to investigate the seasonal variability of the performance of each model. Based on this study, it is expected that PM_{10} estimations using ground-based and satellite-derived AOD data will become an effective approach to monitoring air quality over large spatial domains, especially in complex urban areas.

2 Measurements during the DRAGON-Asia campaign

The study area, Seoul, is a megacity located in a downwind region of northeast Asia, in which air quality is often affected by both pollutants transported over long distances from continental interior and locally generated aerosol. The present study used the column aerosol optical properties measured at 10 Aerosol Robotic Network (AERONET) sites in Seoul, as well as those obtained by a dense mesoscale network of ground-based instruments during the DRAGON-Asia 2012 campaign, which was conducted over the 3-month period March–May 2012 (Fig. 1). The hourly-averaged PM_{10} concentrations were also measured at 10 sites operated by a national air quality monitoring network during the campaign (http://www.airkorea.or.kr).

2.1 Column AOD and surface PM measurements

The AERONET sun photometers (http://aeronet.gsfc.nasa.gov/index.html), which provide aerosol optical and microphysical properties based on direct sun and diffuse sky measurements (Holben et al., 1998), have been widely used as references for measurements from different satellite platforms. The AOD and the Ångström exponent (AE) can be retrieved from direct sun measurements in several spectral bands, usually between 340 and 1020 nm (Holben et al., 1998). Diffuse sky measurements, which are performed at a minimum of four wavelengths (440, 670, 870, and 1020 nm), use an inversion method to provide detailed aerosol properties, such as the size distribution, phase function, single scattering albedo, refractive index, etc. (Holben et al., 1998; Dubovik and King, 2000). The AOD at 550 nm was obtained from AERONET level 2.0 direct sun measurements (cloud-screened and quality-assured) at seven sites, and level 1.5 products (cloud-screened) at three sites. In addition to the AERONET AOD, the effective radius for the total (fine and coarse modes) size distribution obtained from the inversion product was also used to represent the aerosol size information in the empirical regression models (Dubovik and King, 2000). Although cloud-screened AERONET data were used, additional cloud screening was performed for further quality control using the cloud amount data provided by the Korea Meteorological Administration (KMA; http://www.kma.go.kr) and the attenuated backscattering signal measured from the two-wavelength Mie lidar located at Seoul National University (SNU). A cloud-free sky condition was defined as a cloud amount of less than 20 % (cf. Ogunjobi et al., 2004) and no detections of strong scattering peaks of lidar measurements due to clouds. AOD measurements from the Moderate-Resolution Imaging Spectroradiometer (MODIS) onboard the Terra and Aqua satellites

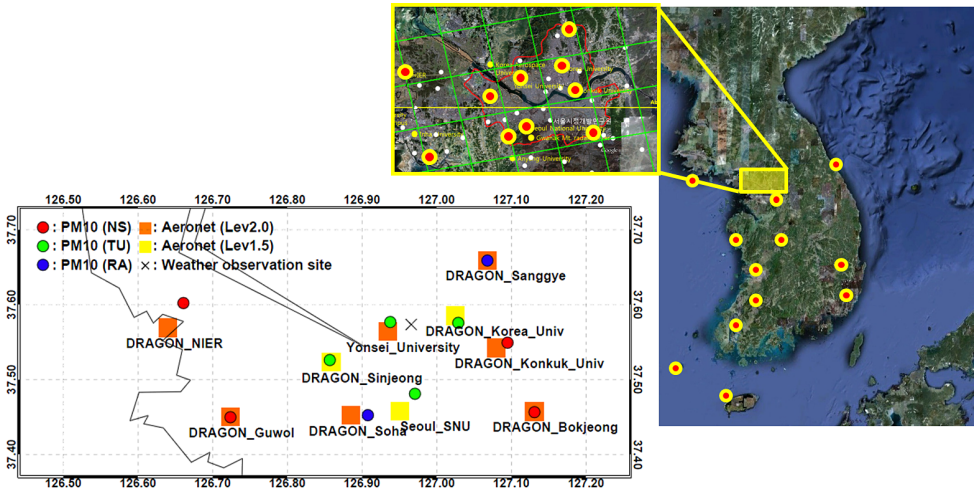

Figure 1. The spatial distribution of AERONET stations, PM_{10} monitoring sites, and weather observation sites across the Seoul metropolitan area. Orange and yellow boxes indicate the locations of AERONET level 2.0 and 1.5 sites, respectively. The colored circles denote the locations of PM_{10} monitoring sites. Red, green, and blue sites represent near-source (NS), typical urban (TU), and residential area (RA) site types, respectively.

were also used to formulate the empirical regression models (Remer et al., 2005; Levy et al., 2007). To identify the optimal grid size for the MODIS AOD in this mesoscale spatial domain, the collocation criteria of the MODIS 550 nm AOD products collected at spatial resolutions of 10 and 30 km were tested and compared with averaged AERONET 550 nm AOD measurements within ±30 min of the satellite overpassing time. As shown in Fig. 2, the MODIS and AERONET AOD data are highly correlated, showing a correlation coefficient (R) greater than 0.85 at most AERONET sites during the DRAGON-Asia campaign. At all AERONET sites except the DRAGON_NIER station, higher correlations between AERONET and MODIS data were found for MODIS resolutions of 10 km than for those with MODIS resolutions of 30 km.

The MODIS AOD data at a 10 km resolution at nadir ("Optical_Depth_Land_And_Ocean") obtained from MODIS Collection 5 aerosol products were also screened out when the MODIS cloud fraction over land ("Cloud_Fraction_Land") was higher than 0.5 or the cloud amount from the KMA was higher than 20 %. Table 2 shows a statistical summary of the AERONET and MODIS AOD data that were available at the measurement sites for the entire campaign period before and after additional cloud screening. The maximum AERONET AOD was reduced by 1.57 (from 2.99 to 1.42) after additional cloud screening, while that of MODIS did not change. The mean and median AERONET AOD values were also reduced after cloud screening, and those of MODIS changed slightly. Also, the number of data sets after cloud screening was reduced by approximately 38.0 %, and the reduction in the available MODIS data after cloud screening was 13.7 %.

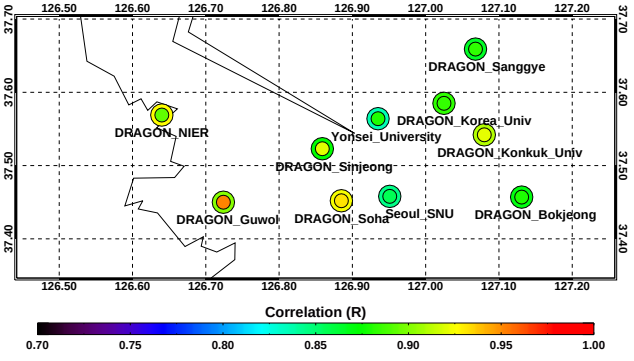

Figure 2. The distribution of correlation coefficients between AERONET AOD and MODIS AOD at 0.55 μm with respect to different spatial resolutions. The inner (outer) circle indicates the correlation between AERONET AOD and MODIS AOD with a resolution of 10 km (30 km).

Hourly-averaged PM_{10} concentrations, measured routinely at 10 national air quality monitoring sites, were used during the DRAGON-Asia campaign. The PM_{10} concentrations were measured by a beta (β)-ray absorption method using a PM_{10} Beta Gauge (model PM_{10}B.G, W&A Inc.), which operates on the premise that the absorption of beta rays increases in proportion to the number of particles collected in the filter (Hauck et al., 2004).

To investigate the relationship between columnar AOD and surface-level PM_{10}, the measurements must be collocated both spatially and temporally. The AERONET AOD data obtained from the station nearest to the PM monitoring site (within a maximum distance of approximately 4.5 km) were used. On the other hand, the MODIS AOD data, which

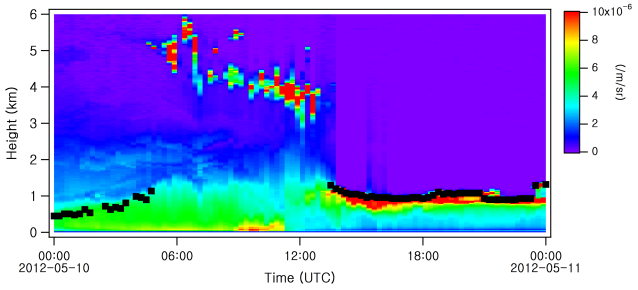

Figure 3. Time plot of attenuated backscatter coefficients observed from the two-wavelength Mie lidar at Seoul National University, and boundary layer height (marked by black squares) retrieved by the automated wavelet covariance transform (WCT) method of Brooks (2003).

Table 2. Statistical summary of AOD and cloud-screened AOD (AOD_{cl}) observed by AERONET and MODIS during the DRAGON-Asia campaign period.

	AERONET		MODIS	
	AOD	AOD_{cl}	AOD	AOD_{cl}
Mean ± SD	0.51 ± 0.34	0.42 ± 0.26	0.74 ± 0.38	0.73 ± 0.37
Min	0.09	0.09	0.03	0.03
Median	0.43	0.35	0.72	0.68
Max	2.99	1.42	1.94	1.94
N	3406	2112	292	252

were measured at different spatial grid resolutions, were extracted within a maximum distance of 0.2° of the PM_{10} measurement sites. The AERONET and MODIS AOD were both temporally collocated within ±30 min of the hourly PM_{10} measurement time.

2.2 Meteorological measurements

Meteorological data were used to investigate the relationship between AOD and PM_{10} concentrations. The attenuated backscatter coefficient at 532 nm, measured by the two-wavelength Mie lidar located at Seoul National University (http://www-lidar.nies.go.jp/Seoul/), was used to calculate the hourly BLH using the automated wavelet covariance transform (WCT) method (Brooks, 2003). The WCT method was applied to backscattered lidar signals at heights above 300 m from the surface to avoid the problem of uncertainty in lidar overlap (Campbell et al., 2002). Figure 3 shows an example of temporal variation in the BLH obtained by application of the WCT method.

In addition to the BLH, other meteorological data such as temperature, relative humidity, cloud amount, and wind speed and direction were obtained from hourly measurements at a KMA weather observation station in Seoul (37.57° N, 126.97° E). All meteorological data within ± 30 min of the PM_{10} observation time were used for this investigation.

3 Methodology

3.1 Relationship between column AOD and surface PM concentration

The AOD is the integration of the radiative extinction due to aerosols from the surface up to the top of the atmosphere (TOA) at a given wavelength. The AOD can be defined as (Koelemeijer et al., 2006)

$$\begin{aligned} \mathrm{AOD} &= \pi \int_0^H \int_0^\infty Q_{\mathrm{ext,amb}}(m,r,\lambda) n_{\mathrm{amb}}(r,z) r^2 \mathrm{d}r\mathrm{d}z \\ &= \pi f(\mathrm{RH}) \int_0^H \int_0^\infty Q_{\mathrm{ext}}(m,r,\lambda) n(r,z) r^2 \mathrm{d}r\mathrm{d}z, \end{aligned} \quad (1)$$

where $Q_{\mathrm{ext,amb}}(m,r,\lambda)$ is the unitless extinction efficiency influenced by the refractive index (m), particle radius (r), and wavelength (λ) under ambient conditions; $Q_{\mathrm{ext}}(m,r,\lambda)$ the extinction efficiency under dry conditions; $n_{\mathrm{amb}}(r,z)$ the size distribution under ambient conditions representing the number of aerosols at corresponding height (z) with a radius (r); $n(r,z)$ the size distribution under dry conditions; and H the top height for the integration.

The PM_{10} concentration, which is the mass concentration of surface-level aerosols with diameters less than 10 µm in dry conditions, is given by

$$\mathrm{PM}_{10} = \frac{4}{3}\pi\rho \int_0^5 r^3 n(r)\mathrm{d}r, \quad (2)$$

where ρ is the particle mass density and r is the dry aerosol radius. With the assumption of a homogeneous aerosol distribution within the BLH, the integration from the surface up to the TOA (H) can be simplified by multiplying by the BLH. Also, the ambient environmental condition can be converted into the dry condition by using the particle hygroscopic growth factor, $f(\mathrm{RH})$. By combining Eqs. (1) and (2), the PM_{10} concentration can be expressed as

$$\mathrm{PM}_{10} = \frac{\mathrm{AOD}}{\mathrm{BLH}\cdot f(\mathrm{RH})} \frac{4\rho R_{\mathrm{eff}}}{3\langle Q_{\mathrm{ext}}\rangle}, \quad (3)$$

where the effective radius R_{eff} and the average of the extinction efficiency over the size distribution $< Q_{\mathrm{ext}} >$ are defined as

$$R_{\mathrm{eff}} = \frac{\int r^3 n(r)\mathrm{d}r}{\int r^2 n(r)\mathrm{d}r}, \langle Q_{\mathrm{ext}}\rangle = \frac{\int r^2 Q_{\mathrm{ext}}(r) n(r)\mathrm{d}r}{\int r^2 n(r)\mathrm{d}r}.$$

In order to extend this analysis to the $PM_{2.5}$, the upper size limit in the integral in Eq. (2) needs to be corrected and fine-mode fraction (FMF) to be additionally considered in Eq. (3). However, since available $PM_{2.5}$ measurements were

Table 3. The empirical linear models used for PM_{10} estimations in this study.

Model	Model description	Application
M1	$PM_{10} = a\,AOD + b$	AERONET, MODIS
M2	$PM_{10} = a\frac{AOD}{BLH} + b$	AERONET, MODIS
M3	$PM_{10} = a\frac{AOD \times R_{eff}}{BLH} + b$	AERONET
M4	$PM_{10} = a\frac{AOD}{BLH \times f(RH)} + b$	AERONET, MODIS
M5	$PM_{10} = a\frac{AOD \times R_{eff}}{BLH \times f(RH)} + b$	AERONET
M6	Sect. 3.2, Eq. (5) (multiple linear regression model)	AERONET

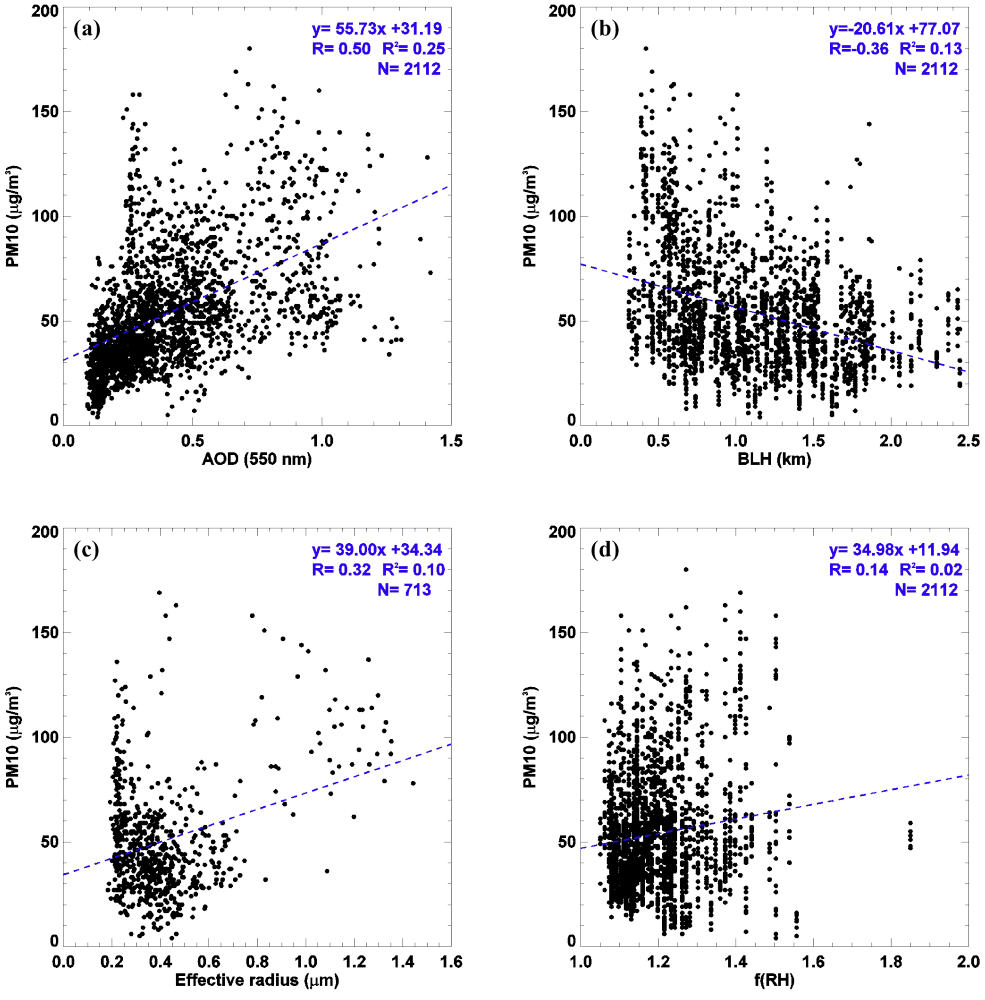

Figure 4. Scatterplots of the various parameters – including **(a)** AOD, **(b)** BLH, **(c)** effective radius, and **(d)** RH – against the dependent variable of PM_{10} concentration. The regression line is shown as a blue dashed line.

quite limited in this area and time, we focused only on PM_{10} in this present study. In Eq. (3), various physical parameters are involved in the relationship between AOD and PM_{10}. The PM_{10} concentration is proportional to AOD, R_{eff}, and particle mass density ρ; on the other hand, PM_{10} is inversely proportional to BLH, $f(RH)$, and $<Q_{ext}>$. To gain insight into the relationship between PM_{10} and major predictors, all PM_{10} concentration was plotted against AOD, BLH, RH, and R_{eff}, which were used in this study for development and validation of the PM_{10} estimation as shown in Fig. 4. The cor-

relation coefficient (R) between PM_{10} and AOD was 0.5, and that of R_{eff} was 0.32. As expected, BLH showed negative correlation with PM_{10} (-0.36). However, RH did not show any significant relationship with PM_{10}. Among these parameters, BLH and $f(\text{RH})$ have been used as parameters in empirical models to estimate PM concentrations using AOD data, as described in Table 1. On the other hand, parameters such as ρ, R_{eff}, and $<Q_{\text{ext}}>$ have been rarely included in empirical models. In the present study, the effective radius of the aerosol size distribution was included for the first time as an additional parameter in the empirical models. The empirical models, and the parameters considered in those models, are described in detail in Sect. 3.2.

3.2 Description of empirical linear models for PM_{10} estimation

Table 3 presents a summary of the various models used in this study. Models M1 to M5 are empirical models based on the relationship between AOD and PM concentration, as described in Sect. 3.1, whereas M6 represents a multiple linear regression model. Among the empirical models, M1, M2, and M4 have been used in previous studies (e.g., Chu et al., 2003; Wang and Christopher, 2003; Engel-Cox et al., 2004, 2006; Koelemeijer et al., 2006; Gupta and Christopher, 2008; Schaap et al., 2009; Emili et al., 2010; Wang et al., 2010). Model M1 includes only AOD as a predictor of the PM_{10} concentration, while M2 additionally includes BLH to consider the aerosol vertical extension. The vertical correction on AOD is represented in M2 by dividing AOD by BLH, with the assumption that aerosols within the boundary layer are homogeneously mixed. Model M4 corrects for RH by using an aerosol hygroscopic growth factor term $f(\text{RH})$ which represents the effects of aerosol hygroscopic growth caused by variations in relative humidity, in addition to the parameters in M2. In this study, $f(\text{RH})$ based on experimental data obtained near the Beijing megacity during the spring was employed (Pan et al., 2009), which is appropriate to this study with respect to both temporal and spatial conditions. Models M3 and M5, which also included the parameters used in M1, M2, and M4, were the first empirical models to include the effective radius of the aerosol size distribution as a size correction factor. Model M3 includes the aerosol effective radius in addition to the parameters in M2 to account for the size of aerosol particles. Model M5 reflects all parameters, including AOD, $f(\text{RH})$, BLH, and the effective radius, as shown in Table 3. The effective radius of the aerosol size distribution for the total mode, which was used in M3 and M5, was obtained from AERONET inversion products (Dubovik and King, 2000; Dubovik et al., 2000). This R_{eff} is one of the main features derived by the particle volume size distribution retrieved by the AERONET inversion algorithm, which was demonstrated to be adequate in practically all situations, especially for the intermediate particle size range ($0.1 \le r \le 7\,\mu\text{m}$) with 10–35 % of retrieval errors, as reported by Dubovik et al. (2002).

In addition to the simple empirical models (M1–M5) derived from the relationship between AOD and PM (Eq. 3), a multiple linear regression (MLR) model was used as a statistical approach to determine PM_{10} concentrations as a function of eight different parameters associated with PM estimation:

$$\begin{aligned}[\text{PM}_{10}] &= \exp(\beta_0) \times (\text{AOD})^{\beta_{\text{AOD}}} (\text{BLH})^{\beta_{\text{BLH}}} (\text{AE})^{\beta_{\text{AE}}} \\ &\times \exp[\beta_{\text{loc}}(\text{Location}) + \beta_{\text{WS}}(\text{WS}) + \beta_{\text{WD}}(\text{WD}) \\ &+ \beta_{\text{RH}}(\text{RH}) + \beta_{\text{Temp}}(\text{Temp})]. \end{aligned} \quad (4)$$

This MLR model of Eq. (4) can be log-transformed into a simpler form of linear regression as shown in Eq. (5).

$$\begin{aligned}\ln[\text{PM}_{10}] &= \beta_0 + \beta_{\text{AOD}} \ln(\text{AOD}) + \beta_{\text{BLH}} \ln(\text{BLH}) \\ &+ \beta_{\text{AE}} \ln(\text{AE}) + \beta_{\text{loc}}(\text{Location}) + \beta_{\text{WS}}(\text{WS}) + \beta_{\text{WD}}(\text{WD}) \\ &+ \beta_{\text{RH}}(\text{RH}) + \beta_{\text{Temp}}(\text{Temp}) \end{aligned} \quad (5)$$

The dependent variable in Eq. (5) is the logarithm of the hourly PM_{10} concentration measured at the PM monitoring sites. The independent variables include aerosol optical properties such as AOD and AE; various meteorological measurements such as BLH, temperature (Temp), and wind speed (WS); and two categorical variables: type of measurement site (Location) and wind direction (WD). The R_{eff} inversion product is from diffuse sky radiance measurement which has strict stability criteria. Thus, the number of data ($N = 713$) is quite lower than products from direct sun measurements including AE ($N = 2112$), which also implies the aerosol size information. For that reason, AE was used as a variable in the MLR model instead of R_{eff} to secure a sufficient number of data samples (Dubovik et al., 2000; Schuster et al., 2006). Measurement sites were categorized into three types: near source (NS), typical urban (TU), and residential area (RA), as shown in Fig. 1. The NS sites were those located within 500 m of sources; sources in this case included traffic-congested roads and industrial complexes. The TU sites were located more than 500 m from sources, in either commercial or residential areas. The RA sites were located more than 500 m from sources and in residential areas only. Wind directions were classified as east, south, west, or north. Regression coefficients (β) were determined for each of the independent variables. This MLR analysis was conducted using the AERONET data set only, because this was sufficient to yield credible results.

For an unbiased assessment of model performance, the entire AERONET data set was randomly divided into two groups, a modeling group ($N = 1058$ for M1, M2, M4, and M6, and $N = 369$ for M3 and M5) that was used to develop the empirical models, and a validation group ($N = 1054$ for M1, M2, M4, and M6, and $N = 373$ for M3 and M5) that was used to validate these models. To minimize the effects of temporal autocorrelation, data were selected such that the time

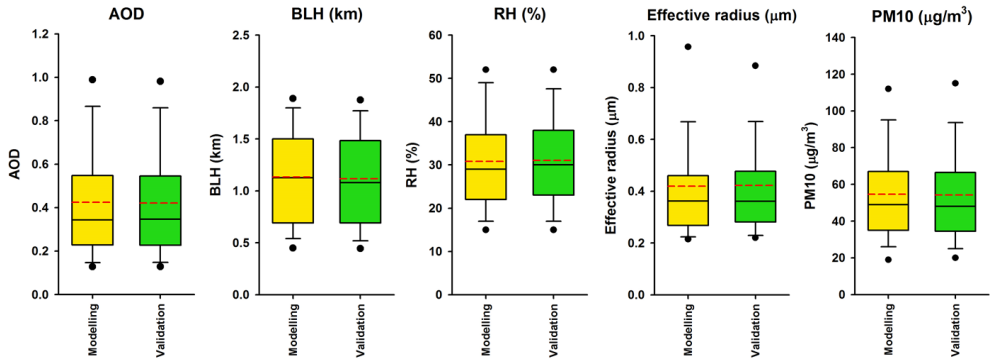

Figure 5. The distribution (5, 10, 25 %, median, 75, 90, and 95 %) of AOD, boundary layer height (BLH), relative humidity (RH), effective radius, and PM_{10} concentrations in the modeling and validation groups derived from AERONET data sets collected during the DRAGON-Asia campaign in Seoul. The red dashed line in the plot denotes the mean value.

Table 4. Estimated regression coefficients for the multiple linear regression model (M6) (described in Sect. 3.2, Eq. 5) using AERONET data ($N = 1058$).

Model parameter	Estimate	Standard error	P value
Intercept	4.363	0.080	< 0.0001
ln(AOD)	0.527	0.022	< 0.0001
ln(BLH)	−0.280	0.028	< 0.0001
ln(AE)	0.066	0.033	0.047
Location type			
Near source	0.233	0.032	< 0.0001
Urban	0.013	0.032	0.684
Suburban	0.000	–	–
Wind speed	0.015	0.008	0.052
Wind direction			
From the north	0.205	0.054	< 0.0001
From the south	0.164	0.045	< 0.0001
From the west	0.307	0.036	< 0.0001
From the east	0.000	–	–
RH	−0.610	0.116	< 0.0001
Temperature	−0.010	0.002	< 0.0001

interval between validation and modeling data was at least 24 h. Summary statistics for the variables involved in the modeling and validation data sets are shown in Fig. 5. All empirical models for hourly PM_{10} estimates based on the AERONET data sets were fitted using the modeling data set to estimate the model coefficients. Estimated regression coefficients (β), standard errors, and p values of parameters used in M6 (Eq. 5) are summarized in Table 4. As shown in Table 4, most parameters used in M6 were found to be highly significant ($p < 0.0001$) predictors of the PM_{10} concentration. The positive sign of the coefficient for AOD (0.527 ± 0.022) shows a direct correspondence between AOD and surface PM_{10}, given that other conditions remained constant. On the other hand, the estimated power of the BLH relationship was negative (-0.280 ± 0.028), which indicates an inverse relationship between BLH and the PM_{10} concentration. The reason for this inverse relationship is that a lower BLH confines aerosols to a thinner atmospheric layer, resulting in higher surface PM_{10} concentrations. A negative coefficient was also obtained for RH (-0.610 ± 0.116), showing that higher RH conditions result in lower PM_{10} concentrations (given constant AOD values) – i.e., the effect of aerosol hygroscopic growth is reflected in the MLR model (M6).

In this analysis, MODIS data sets collected over Seoul during the DRAGON-Asia campaign were not divided into two groups (for model development and validation) due to the relatively small size of the MODIS data set obtained during the campaign ($N = 252$ for M2 and M4, as compared with $N = 1054$ for M2 and M4 for the AERONET data set).

4 Results and discussion

4.1 Evaluation of estimated PM_{10} using various empirical linear models

The hourly PM_{10} concentrations estimated by the various empirical models were evaluated by comparing them with measured hourly surface-level PM_{10}. Table 5 shows a summary of the correlations and statistics between the measured and estimated PM_{10} concentrations using the various model types, obtained using the AERONET and MODIS data sets. The simplest model (M1), with only AOD as a predictor, yields the lowest correlation of 0.40 (0.46) using the AERONET (MODIS) data set for the PM_{10} estimation. The correlation obtained using the cloud-screened AOD data ($M1_{cl}$) is higher than that obtained using the raw AOD data (M1), which implies that cloud screening contributes

Table 5. Correlation coefficient (R), root mean square error (RMSE), mean normalized bias (MNB), and mean fractionalized bias (MFB) between measured PM_{10} concentrations and those estimated by the different empirical linear models, using AERONET and MODIS data, during the DRAGON-Asia campaign period in Seoul. Numbers in parentheses represent results corresponding to the same number of data points as used in M3 and M5, when effective radius of aerosol data were available.

		Model						
		M1	$M1_{cl}$	M2	M3	M4	M5	M6
AERONET	R	0.40	0.54	0.62 (0.46)	0.55	0.63 (0.47)	0.58	0.68
	R^2	0.16	0.29	0.39 (0.21)	0.30	0.40 (0.23)	0.34	0.47
	N	1712	1054	1054 (373)	373	1054 (373)	373	1054
	RMSE ($\mu g\,m^{-3}$)[a]	28.62	23.79	22.11 (23.27)	22.01	22.11 (22.98)	21.32	21.05
	MNB (%)[b]	27.70	21.75	21.27 (25.39)	22.11	21.27 (24.54)	20.66	5.65
	MFB (%)[c]	10.96	9.20	8.97 (10.43)	9.08	8.97 (10.17)	8.50	−0.83
MODIS	R	0.46	0.50	0.72	–	0.71	–	–
	R^2	0.21	0.25	0.51	–	0.51		
	N	291	252	252	–	252	–	–
	RMSE ($\mu g\,m^{-3}$)	28.49	28.55	23.02	–	23.19	–	–
	MNB (%)	22.09	21.83	14.80	–	14.92	–	–
	MFB (%)	9.53	9.64	6.40	–	6.53	–	–

[a] RMSE (root mean square error) $= \sqrt{\frac{1}{N}\sum_{i=1}^{N}(m_i - o_i)^2}$;

[b] MNB (mean normalized bias) $= \frac{1}{N}\sum_{i=1}^{N}\frac{(m_i - o_i)}{o_i} \times 100\,\%$;

[c] MFB (mean fractionalized bias) $= \frac{1}{N}\sum_{i=1}^{N}\frac{(m_i - o_i)}{\left(\frac{m_i + o_i}{2}\right)} \times 100\,\%$;

m_i and o_i indicate estimated PM_{10} using models and observed PM_{10} concentrations, respectively. N is the number of data points.

to an increase in the correlation between measured PM and AOD by removing overestimated AOD measurements resulting from cloud contamination (e.g. Schaap et al., 2009).

Model M2, in which BLH is an added parameter, shows a correlation coefficient of 0.62 (0.72) and a root mean square error (RMSE) of 22.11 (23.02) $\mu g\,m^{-3}$ between measured and estimated PM_{10} using the AERONET (MODIS) AOD data; in this case, the estimate using MODIS AOD data as an input is a better predictor than the estimate obtained using the AERONET data (Table 5). This higher performance of the MODIS AOD and model M2 can be attributed to a MODIS overpass time near midday, when aerosols are generally well mixed in the boundary layer, as compared with the situation in the early morning or late afternoon. These improved correlation coefficients imply that a vertical correction on AOD using the BLH value improves PM_{10} estimates. The correlations between measured and estimated PM_{10} using M2 with MODIS data are slightly higher than those obtained in the previous work of Emili et al. (2010), which was based on a combination of Spinning Enhanced Visible and Infrared Imager (SEVIRI) and MODIS AOD data to estimate hourly PM_{10} concentrations over the European Alpine regions. The differences between the results of Emili et al. (2010) and those obtained here could be associated with uncertainties in surface reflectance in Alpine regions that resulted in relatively larger errors in the Alpine AOD data as compared with those obtained in Seoul.

Aerosol effective radius data obtained from AERONET measurements was used as a parameter in model M3 to estimate PM_{10}. The effective radius of aerosol, as derived from sky radiances obtained from solar almucantar measurements, is available only when the solar zenith angle (SZA) is larger than 50° (except for near local noon), which avoids polarization effects (Holben et al., 1998; Dubovik and King, 2000). Consequently, in contrast to the AOD data, the effective radius data are available only in a limited time window. The limited number of effective radius measurements was used as an input to M3 to estimate PM_{10}; we used 35.4 % ($N = 373$) of the total number of AERONET validation data sets ($N = 1054$) in which data were simultaneously available for both AOD and the effective radius. Model M3 was not implemented using MODIS AOD due to a lack of effective radius information in the MODIS data sets over land areas. As shown in Table 5, the correlation between measured PM_{10} and those estimated from M3 is higher than that obtained using M2 with the same number of data sets ($N = 373$; $R_{M3,AERO} = 0.55$, $R_{M2,AERO} = 0.46$). Although the results are subject to further validation, aerosol size corrections using the effective radius (M3), in general, lead to better estimates of PM_{10} concentrations than do those without (M2), at least during the time frame of the intensive campaign period.

Model M4, which incorporates the aerosol hygroscopic growth factor ($f(RH)$) in PM_{10} estimation, yields a correlation coefficient of 0.63 (0.71) for the AERONET (MODIS)

Table 6. Spatial variations of the correlation coefficient (R), root mean square error (RMSE), mean normalized bias (MNB), and mean fractionalized bias (MFB) between measured PM_{10} concentrations and those estimated from the different empirical linear models for the three different site categories, using the data collected by AERONET and MODIS, during the DRAGON-Asia campaign period in Seoul.

Performance of empirical models used to estimate hourly PM_{10} using AERONET data sets with respect to model and measurement site types							
		Model					
		$M1_{cl}$	M2	M3	M4	M5	M6
NS	R	0.49	0.57 (0.49)	0.59	0.57 (0.49)	0.61	0.61
	R^2	0.24	0.32 (0.24)	0.35	0.33 (0.24)	0.38	0.37
	N	807	807 (237)	237	807 (237)	237	190
	RMSE ($\mu g\,m^{-3}$)	26.29	24.79 (26.90)	24.79	24.67 (26.79)	24.28	22.85
	MNB (%)	21.21	20.54 (27.32)	24.57	20.38 (26.95)	23.48	7.12
	MFB (%)	9.03	8.56 (15.21)	13.05	8.65 (15.05)	12.35	−0.37
TU	R	0.51	0.60 (0.43)	0.61	0.61 (0.45)	0.64	0.72
	R^2	0.26	0.36 (0.18)	0.37	0.37 (0.20)	0.42	0.51
	N	891	891 (367)	367	891 (367)	367	190
	RMSE ($\mu g\,m^{-3}$)	22.61	21.11 (21.77)	19.06	20.94 (21.50)	18.43	17.69
	MNB (%)	24.27	24.25 (23.91)	20.26	23.47 (22.67)	18.46	4.16
	MFB (%)	10.09	9.84 (6.14)	5.39	9.88 (5.78)	4.86	−1.85
RA	R	0.63	0.73 (0.63)	0.69	0.73 (0.64)	0.70	0.76
	R^2	0.40	0.53 (0.40)	0.47	0.54 (0.42)	0.50	0.59
	N	414	414 (109)	109	414 (109)	109	92
	RMSE ($\mu g\,m^{-3}$)	19.67	17.35 (18.02)	16.92	17.26 (17.81)	16.53	17.09
	MNB (%)	17.31	16.08 (25.85)	22.60	15.32 (25.19)	21.52	5.99
	MFB (%)	8.15	7.26 (13.61)	12.08	6.94 (13.41)	11.62	0.47
Performance of empirical models to estimate hourly PM_{10} using MODIS data sets with respect to model and measurement site types							
		Model					
		$M1_{cl}$	M2	M3	M4	M5	M6
NS	R	0.37	0.68	–	0.68	–	–
	R^2	0.14	0.46	–	0.46	–	–
	N	105	105	–	105	–	–
	RMSE ($\mu g\,m^{-3}$)	32.09	27.34	–	27.32	–	–
	MNBE (%)	24.93	16.10	–	15.98	–	–
	MFB (%)	10.80	6.99	–	7.04	–	–
TU	R	0.42	0.72	–	0.71	–	–
	R^2	0.18	0.52	–	0.50	–	–
	N	95	95	–	95	–	–
	RMSE ($\mu g\,m^{-3}$)	26.41	20.08	–	20.45	–	–
	MNBE (%)	21.23	15.23	–	15.58	–	–
	MFB (%)	9.42	6.55	–	6.78	–	–
RA	R	0.50	0.76	–	0.74	–	–
	R^2	0.25	0.57	–	0.55	–	–
	N	52	52	–	52	–	–
	RMSE ($\mu g\,m^{-3}$)	23.66	17.93	–	18.33	–	–
	MNBE (%)	17.36	11.40	–	11.57	–	–
	MFB (%)	7.96	4.93	–	5.04	–	–

data set (Table 5). These correlations are similar to those obtained using M2, in which the RH correction is absent. The results suggest that RH levels do not significantly influence BLH-corrected estimates at our measurement sites during the campaign period, during which average daytime RH values were 30.5 ± 11.0 %; at these RH levels, it appears that aerosols are largely unaffected by hygroscopic growth.

The PM_{10} estimates derived from M5 – which considers BLH, f(RH), and the effective radius – were also evaluated by comparisons with PM_{10} concentrations measured at the surface. As discussed previously, the number of samples for the effective radius used in M3 ($N = 373$) was also used in M5, and M5 was also evaluated using the AERONET data. Table 5 shows that the correlation coefficient obtained using model M5 was 0.58, while those from M3 and M4 were 0.55 and 0.47, respectively, using the same number of data sets ($N = 373$). The correlation between measured and estimated PM_{10} concentrations obtained from M5 is higher than that obtained from M4, on account of the addition of aerosol size information. However, this correlation obtained from M5 is slightly improved relative to that obtained from M3, as the effect of the RH correction is considered to be negligible for PM_{10} estimations using data collected during the DRAGON-Asia campaign when average RH values were low.

The PM_{10} concentrations were also estimated from the MLR model (M6). As discussed in Sect. 3.2, 1054 AERONET data sets were used for the validation of PM_{10} estimated using M6. The correlation coefficient between the measured PM_{10} and those estimated from M6 is 0.68. This correlation coefficient is the highest among those obtained by any of the empirical models in this study, and it shows that various meteorological parameters – such as RH, temperature, wind speed, and wind direction – contribute to a substantial increase in the accuracy of PM_{10} estimates.

The BLH and the effective radius of aerosols are the dominant predictors of PM_{10} in the empirical models, while the effect of RH on PM_{10} estimation during the campaign period is negligible. However, the contribution of the RH correction may vary seasonally, which is further discussed in Sect. 4.3. In terms of the errors in the estimated PM_{10} concentrations, the RMSE of PM_{10} estimated using M6 (M2) with the input of the AERONET (MODIS) data set is 21.05 (23.02) $\mu g\,m^{-3}$, which is the lowest among those calculated with the empirical models (Table 5). The RMSE values between measured PM_{10} concentrations and those estimated using $M1_{cl}$ ($N = 1054$), M2 ($N = 1054$), and M4 ($N = 1054$), based on the same number of AERONET data sets as inputs, are 23.79, 22.11, and 22.11 $\mu g\,m^{-3}$, respectively, showing that the models tend to improve (i.e., the errors tend to decrease) when using the BLH as a predictor in the empirical models. This improvement in the models was also found when a vertical correction is applied to the MODIS data. The RMSE values of PM_{10} estimated using $M1_{cl}$ ($N = 252$), M2 ($N = 252$), and M4 ($N = 252$), and based on inputs of MODIS data, were 28.55, 23.02, and 23.19 $\mu g\,m^{-3}$, respectively. The RMSE values of PM_{10} estimated using M2 ($N = 373$), M3 ($N = 373$), and M5 ($N = 373$), and based on the same number of AERONET data sets, were 23.27, 22.01, and 21.32 $\mu g\,m^{-3}$, respectively, when a size correction using the aerosol effective radius and an RH correction using the particle hygroscopic growth factor were incorporated into the models. To evaluate the empirical model performance for PM_{10} estimation, the mean normalized bias (MNB) and the mean fractionalized bias (MFB) were also calculated (these statistical parameters are described in the footnote of Table 5). The tendencies of both the MNB and MFB are similar to those of the RMSE, except for M6. All MFB values (except for M6) are positive, which indicates that the PM_{10} concentrations derived from the models are generally overestimated when compared with measured PM_{10} values. The MFB of M6 was -0.83 %, which shows that M6 tends to underestimate the PM_{10} concentration, especially at high concentrations on account of the log transformation of the data.

4.2 Spatial characteristics of correlations between measured and estimated PM_{10}

Large variations in the mean and standard deviation of the measured PM_{10} concentrations were observed, with the size of the deviations dependent on the measurement site type. As described in Sect. 3.2, the site types include NS, TU, and RA site types in Seoul, as identified during the DRAGON-Asia campaign. The means (standard deviations) of the hourly measured PM_{10} concentration in Seoul during the campaign period were 62.21 (± 33.78), 53.42 (± 28.40), and 52.19 (± 26.15) $\mu g\,m^{-3}$ at the NS, TU, and RA site types, respectively. The highest mean and standard deviation of the PM_{10} concentrations were found at the NS site type, while the lowest were found at the RA site type.

To identify spatial variability within the performance of the empirical models, the correlations between measured and estimated PM_{10} concentrations were further investigated with respect to the classification of site types (NS, TU, and RA). Table 6 shows the correlations between measured and estimated PM_{10}, with inputs of AERONET and MODIS data, and as dependent on the measurement site type. As shown in Table 6, correlation coefficients for the RA site show good model performances (0.69–0.76) using M3, M5, and M6; however, model performances for the NS and TU site types fall within the ranges 0.59–0.61 and 0.61–0.72, respectively. Correlation coefficients for the RA site type are in the range 0.63–0.73 for models $M1_{cl}$, M2, and M4, whereas those for the NS and TU site types are 0.49–0.57 and 0.51–0.61, respectively. The RMSE values are 16.53–19.67, 17.69–22.61, and 22.85–26.79 $\mu g\,m^{-3}$ for the RA, TU, and NS site types, respectively, showing that errors in PM_{10} estimates at NS site types are higher than those at TU and RA site types. Thus, the highest correlation in each empirical model was obtained for the RA sites, while the lowest was found at the NS sites (Table 6). The NS site type shows large spatial and temporal

Table 7. Seasonal variations of the correlation coefficient (R) and root mean square error (RMSE) between measured PM_{10} concentrations and those estimated by the different empirical linear models using AERONET data sets, collected at Yonsei University for 17 months.

Performance of empirical models to estimate hourly PM_{10} using AERONET data sets with respect to model and season						
		Model				
		$M1_{cl}$	M2	M3	M4	M5
Spring	R	0.39	0.47 (0.45)	0.48	0.48 (0.46)	0.54
	R^2	0.15	0.22 (0.20)	0.24	0.23 (0.21)	0.29
	N	465	465 (142)	142	465 (142)	142
	RMSE ($\mu g\,m^{-3}$)	41.17	39.60 (29.39)	28.77	39.37 (29.16)	27.76
Summer	R	0.70	0.67 (0.64)	0.64	0.71 (0.67)	0.66
	R^2	0.50	0.46 (0.41)	0.41	0.50 (0.45)	0.43
	N	85	85 (21)	21	85 (21)	21
	RMSE ($\mu g\,m^{-3}$)	13.85	14.39 (13.75)	13.60	13.81 (13.13)	10.39
Autumn	R	0.60	0.64 (0.52)	0.54	0.66 (0.57)	0.58
	R^2	0.36	0.42 (0.28)	0.29	0.41 (0.33)	0.34
	N	212	212 (99)	99	212 (99)	99
	RMSE ($\mu g\,m^{-3}$)	13.41	12.89 (14.86)	14.71	12.66 (14.32)	14.17
Winter	R	0.63	0.70 (0.70)	0.81	0.70 (0.70)	0.81
	R^2	0.40	0.49 (0.49)	0.65	0.49 (0.49)	0.66
	N	284	284 (116)	116	284 (116)	116
	RMSE ($\mu g\,m^{-3}$)	19.81	18.17 (21.16)	17.44	18.10 (21.01)	17.29

variability in surface PM_{10} concentrations due to large anthropogenic aerosol emissions, which presents difficulties in the development of empirical models for estimating PM_{10} concentrations. The results obtained using the AERONET data (Table 6) also demonstrate that hourly PM_{10} estimations depend largely on both the empirical model used for the estimation and the site type in megacity areas, where the spatial and temporal variability of aerosol concentrations is large.

As discussed in Sect. 4.1, the spatial dependency of empirical model performance using the MODIS data inputs was investigated only for models $M1_{cl}$, M2, and M4, due to a lack of effective radius information in the MODIS data. The spatial dependency of the empirical model performance using the MODIS data is large. Table 6 shows the highest correlations for the RA site type, while the lowest are for the NS sites. The correlation coefficients for the RA sites were between 0.50 and 0.76 for models $M1_{cl}$, M2, and M4, whereas those for the TU and NS sites were 0.42–0.72 and 0.37–0.68, respectively. The highest correlation between measured and estimated PM_{10}, obtained using M2 with MODIS data, was comparable with those obtained using M5 and M6 with AERONET data. This high performance of the empirical models using the MODIS data can be explained by the overpass time of the MODIS data, which was around midday, when aerosols are generally well-mixed within the boundary layer compared with other times of the day (Schaap et al., 2009).

The inverse distance weighting (IDW) interpolation method was applied to estimate the PM_{10} concentrations using M2 with MODIS AOD data over various campaign sites, at a spatial resolution that was finer than that established for the original MODIS data (10 km). The IDW method was used to estimate PM_{10} concentrations in Alpine regions with simple PM source distributions (Emili et al., 2010). In this study, model M2 with MODIS AOD and lidar BLH data was used to estimate PM_{10} concentrations at a resolution of 0.02° (ca. 2 km) over the Seoul area. Slopes and intercepts of M2 were spatially interpolated to a resolution of 0.02° using the IDW method, as calculated from values at the four closest pixels. Figure 6 shows PM_{10} estimates at the 2 km resolution based on the IDW method, where the colored circles represent PM_{10} concentrations measured at PM monitoring sites. The spatial distribution of the estimated and measured PM_{10} concentrations is generally in good agreement. However, a discontinuity is observed in Fig. 6, which could be due to a problem associated with AOD input at a low resolution and its interpolation based on inhomogeneous sampling of a small number of data points. In order to understand smaller-scale features of the air quality, higher spatial resolution AOD products such as a MODIS 3 km product are under development. Although this high-resolution product has been expected to explain aerosol gradients in detail at a small scale, the 3 km product showed poor performances compared to the 10 km product due to improper characteriza-

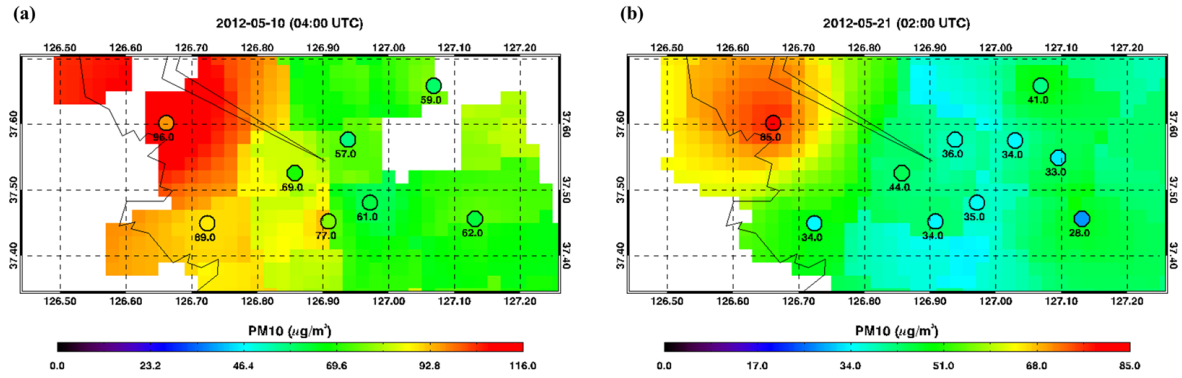

Figure 6. Distribution of hourly surface PM_{10} concentrations estimated by model M2 using the MODIS data sets for **(a)** 04:00 UTC on 10 May 2012 and **(b)** 02:00 UTC on 21 May 2012. Circles indicate the observed PM_{10} concentrations at PM monitoring sites.

tion of the urban surfaces (Levy et al., 2013; Munchak et al., 2013). This bias in surface reflectance of MODIS algorithm indeed resulted in misfit between column AOD and surface PM concentration, as discussed in Escribano et al. (2014). Thus, estimated spatial characteristics of surface PM concentrations are reliable when aerosol products are satisfied with both higher quality and finer resolution.

4.3 Seasonal characteristics of correlations between measured and estimated PM_{10}

The empirical models proposed in Sect. 3.2 were applied to data collected for an extended time period (beyond that of the DRAGON-Asia campaign) at a Yonsei University (YU) site to investigate the seasonal characteristics of the various empirical model performances for PM_{10} estimation. Seasonal effects were studied during all four seasons (spring, summer, autumn, and winter), defined here as the periods March–May, June–August, September–November, and December–February, respectively. The AERONET level 2.0 data were used from March 2011 to July 2012 at the YU site, as YU is the only site in Seoul where AERONET level 2.0 data are available for the period that covers all four seasons, and which also includes the DRAGON-Asia campaign period. All models except for MLR model M6 were used to identify the seasonal dependency of model performance; M6 was not used because the number of data sets was insufficient to determine the regression coefficients for the four different seasons.

Table 7 summarizes the seasonal variations in the correlations between measured and estimated PM_{10} using the various empirical models and the AERONET data. The overall statistics (including correlation coefficients) of the models using the AERONET data were found to be poorest in spring, when compared with those of other seasons. Correlation coefficients using all empirical models and the AERONET data (Table 7) were in the range 0.39–0.54 for spring, whereas those for summer, autumn, and winter were 0.64–0.71, 0.52–0.66, and 0.63–0.81, respectively. The poor performance in spring can be attributed to frequent occurrences of Asian dust events as well as persistent anthropogenic influences at YU which is located in a continental downwind region. The Asian dust events in spring generate inhomogeneous aerosol vertical distributions due to elevated aerosol layers above the BLH, which are not taken into account by using BLH in the empirical models (Murayama et al., 2001; S. W. Kim et al., 2007). Therefore, the performance using M2 in spring ($R = 0.47$) is still much poorer than performances in other seasons ($R \geq 0.64$), which could be attributed to the presence of multiple aerosol layers and mixtures of different types of aerosols in spring.

The highest correlations of estimated and measured PM_{10} concentrations occur in winter using M3 and M5 ($R = 0.81$), which both consider the BLH and the effective radius of aerosol. In winter, a lower aerosol mixing height and homogeneous microphysical and optical properties within the BLH are thought to result in BLH and the effective radius being the dominant predictors in the empirical models for PM_{10} estimation. A lower aerosol mixing height is often induced by a temperature inversion in winter, when homogeneous aerosol properties are likely to be present within the boundary layer due to the reduced influence of the long-range transport of aerosols above the BLH. The correlation using M4, which considers BLH and RH in summer ($N = 85$) and autumn ($N = 212$), when RH is relatively higher than in the other two seasons, yields correlations of 0.71 and 0.66, respectively. In summer, the RH correction improves the PM_{10} estimation, yielding a correlation of 0.71 using M4 compared with a correlation of 0.67 using M2. In autumn, incorporation of the RH correction into the models (M4) yields a slightly improved correlation compared with models that exclude the RH correction (M2); i.e., 0.66 and 0.64, respectively. The correlation also increases from 0.64 (M3) to 0.66 (M5), and from 0.54 (M3) to 0.58 (M5), in summer and autumn, respectively, when including the RH correction, which shows that the RH correction is effective in conditions of higher RH.

5 Conclusions

Concentrations of PM_{10} were estimated in Seoul, Korea, during the DRAGON-Asia campaign period by considering the effective radius of the aerosol size distribution, together with BLH, RH, and AOD, within empirical models that used AERONET data obtained at multiple sites for the first time. The performances of various empirical models were also evaluated for hourly PM_{10} estimations using AERONET and MODIS data sets. The improved performances were found when the vertical correction on AOD using the BLH was applied in both AERONET and MODIS data sets (M2) compared to the simplest model (M1). These empirical model performances were further enhanced by additionally including the effective radius for size correction (M3, M5). However, not meaningful improvements were found when RH was considered additionally (M4). Among different empirical models based on the physical relationship between AOD and PM concentration (M1–M5), model M5, which follows the nearest form of that relationship with the largest number of parameters, showed the best performance. In general, BLH and the effective radius were found to be the key parameters when estimating PM_{10} using the empirical models, while RH did not show any significant effect on PM_{10} estimation using the multiple data sets collected during the spring campaign period, when RH is relatively lower than summer and autumn.

The spatial variability of empirical model performance was also investigated for three different site types, which were categorized according to the distance between sources and instruments. The highest correlation for each empirical model using both AERONET and MODIS data occurred for the RA sites, while the lowest was for the NS sites, where the spatiotemporal variability of aerosols is high. The selection of site types either dominates or is comparable with the specific empirical model selected for estimating PM_{10} concentrations in Seoul, as results are significantly affected by the spatial variability of aerosols. The performances of the models for estimating PM_{10} were also good at midday when aerosols are well mixed within the boundary layer, which suggests a dependence of PM_{10} estimation on the measurement time.

Seasonal variations in the performances of the empirical models for PM_{10} estimation were detected. The highest correlation was found using M3 and M5 in winter ($R = 0.81$), when both BLH and the effective radius of the aerosol are considered; the high correlations can be attributed to a lower aerosol mixing height and homogeneity in the optical and microphysical properties of aerosols within the BLH. The poorest performance was found in spring, when the impact of Asian dust events on both inhomogeneous vertical structure of particle number and aerosol composition at the measurement sites is common, and leads to variable effects.

As discussed in this study, the spatial distribution of surface-level PM_{10} concentrations can be estimated using empirical models. The use of satellite measurements in these various empirical models has the advantage of both simplicity and wide spatial coverage over megacity areas. However, the predictability of PM_{10} distributions using empirical models should be improved. For better estimating surface PM concentrations by satellite remote sensing, especially in urban areas where diverse aerosol sources are distributed, aerosol products with a higher quality and a finer resolution are required. Additionally, accurate and detailed information about aerosol vertical distribution, size distribution, and composition will contribute to improve empirical models. Also, to enhance the accuracy of PM_{10} estimations in other seasons, further work is required to investigate seasonal effects on the spatial variability of PM_{10} estimations in Seoul. In addition to the evaluation of multiple empirical models in the megacity area, a CTM should also be performed and validated for PM_{10} estimations.

Acknowledgements. This research was supported by the GEMS program of the Ministry of Environment, Korea, and the Eco Innovation Program of KEITI (2012000160002). The authors deeply appreciate NIER and the staff for the DRAGON-Asia campaign in establishing and maintaining the AERONET sites. We would also like to thank NIER for the PM_{10} data used, NASA for the AERONET and MODIS data, and NIES Lidar team for the lidar data. This research was partially supported by the Brain Korea 21 Plus Program for S. Seo, J. Kim, H. Lee, U. Jeong, and W. Kim.

Edited by: P. Quinn

References

Baumer, D., Vogel, B., Versick, S., Rinke, R., Mohler, O., and Schnaiter, M.: Relationship of visibility, aerosol optical thickness and aerosol size distribution in an ageing air mass over South-West Germany, Atmos. Environ., 42, 989–998, doi:10.1016/j.atmosenv.2007.10.017, 2008.

Brauer, M., Amann, M., Burnett, R. T., Cohen, A., Dentener, F., Ezzati, M., Henderson, S. B., Krzyzanowski, M., Martin, R. V., and Van Dingenen, R.: Exposure assessment for estimation of the global burden of disease attributable to outdoor air pollution, Environ. Sci. Technol., 46, 652–660, 2012.

Brook, R. D., Rajagopalan, S., Pope, C. A., Brook, J. R., Bhatnagar, A., Diez-Roux, A. V., Holguin, F., Hong, Y. L., Luepker, R. V., Mittleman, M. A., Peters, A., Siscovick, D., Smith, S. C., Whitsel, L., Kaufman, J. D., Epidemiol, A. H. A. C., Dis, C. K. C., and Metab, C. N. P. A.: Particulate Matter Air Pollution and Cardiovascular Disease An Update to the Scientific Statement From the American Heart Association, Circulation, 121, 2331–2378, 2010.

Brooks, I. M.: Finding boundary layer top: Application of a wavelet covariance transform to lidar backscatter profiles, J. Atmos. Ocean. Tech., 20, 1092–1105, 2003.

Campbell, J. R., Hlavka, D. L., Welton, E. J., Flynn, C. J., Turner, D. D., Spinhirne, J. D., Scott, V. S., and Hwang, I. H.: Full-time,

eye-safe cloud and aerosol lidar observation at atmospheric radiation measurement program sites: Instruments and data processing, J. Atmos. Ocean. Tech., 19, 431–442, 2002.

Choi, Y. S., Park, R. J., and Ho, C. H.: Estimates of ground-level aerosol mass concentrations using a chemical transport model with Moderate Resolution Imaging Spectroradiometer (MODIS) aerosol observations over East Asia, J. Geophys. Res.-Atmos., 114, D04204, doi:10.1029/2008JD011041, 2009.

Chu, D. A., Kaufman, Y. J., Zibordi, G., Chern, J. D., Mao, J., Li, C. C., and Holben, B. N.: Global monitoring of air pollution over land from the Earth Observing System-Terra Moderate Resolution Imaging Spectroradiometer (MODIS), J. Geophys. Res.-Atmos., 108, 4661, doi:10.1029/2002jd003179, 2003.

Dubovik, O., Holben, B. N., Eck, T. F., Smirnov, A., Kaufman, Y. J., King, M. D., Tanré, D., and Slutsker, I.: Variability of absorption and optical properties of key aerosol types observed in worldwide locations, J. Atmos. Sci., 59, 590–608, 2002.

Dubovik, O., Smirnov, A., Holben, B., King, M. D., Kaufman, Y. J., Eck, T. F., and Slutsker, I.: Accuracy assessments of aerosol optical properties retrieved from Aerosol Robotic Network (AERONET) Sun and sky radiance measurements, J. Geophys. Res.-Atmos., 105, 9791–9806, 2000.

Dubovik, O. and King, M. D.: A flexible inversion algorithm for retrieval of aerosol optical properties from Sun and sky radiance measurements, J. Geophys. Res.-Atmos., 105, 20673–20696, doi:10.1029/2000jd900282, 2000.

Dubovik, O., Smirnov, A., Holben, B. N., King, M. D., Kaufman, Y. J., Eck, T. F., and Slutsker, I.: Accuracy assessments of aerosol optical properties retrieved from Aerosol Robotic Network (AERONET) Sun and sky radiance measurements, J. Geophys. Res.-Atmos., 105, 9791–9806, doi:10.1029/2000jd900040, 2000.

Emili, E., Popp, C., Petitta, M., Riffler, M., Wunderle, S., and Zebisch, M.: PM_{10} remote sensing from geostationary SEVIRI and polar-orbiting MODIS sensors over the complex terrain of the European Alpine region, Remote Sens. Environ., 114, 2485–2499, doi:10.1016/j.rse.2010.05.024, 2010.

Engel-Cox, J. A., Holloman, C. H., Coutant, B. W., and Hoff, R. M.: Qualitative and quantitative evaluation of MODIS satellite sensor data for regional and urban scale air quality, Atmos. Environ., 38, 2495–2509, doi:10.1016/j.atmosenv.2004.01.039, 2004.

Engel-Cox, J. A., Hoff, R. M., Rogers, R., Dimmick, F., Rush, A. C., Szykman, J. J., Al-Saadi, J., Chu, D. A., and Zell, E. R.: Integrating lidar and satellite optical depth with ambient monitoring for 3-dimensional particulate characterization, Atmos. Environ., 40, 8056–8067, doi:10.1016/j.atmosenv.2006.02.039, 2006.

Escribano, J., Gallardo, L., Rondanelli, R., and Choi, Y.-S.: Satellite retrievals of aerosol optical depth over a subtropical urban area: the role of stratification and surface reflectance, Aerosol. Air. Qual. Res., 14, 596–568, 2014.

Guo, J.-P., Zhang, X.-Y., Che, H.-Z., Gong, S.-L., An, X., Cao, C.-X., Guang, J., Zhang, H., Wang, Y.-Q., and Zhang, X.-C.: Correlation between PM concentrations and aerosol optical depth in eastern China, Atmos. Environ., 43, 5876–5886, 2009.

Gupta, P. and Christopher, S. A.: Seven year particulate matter air quality assessment from surface and satellite measurements, Atmos. Chem. Phys., 8, 3311–3324, doi:10.5194/acp-8-3311-2008, 2008.

Hauck, H., Berner, A., Gomiscek, B., Stopper, S., Puxbaum, H., Kundi, M., and Preining, O.: On the equivalence of gravimetric PM data with TEOM and beta-attenuation measurements, J. Aerosol Sci., 35, 1135–1149, doi:10.1016/j.aerosci.2004.04.004, 2004.

Holben, B. N., Eck, T. F., Slutsker, I., Tanre, D., Buis, J. P., Setzer, A., Vermote, E., Reagan, J. A., Kaufman, Y. J., Nakajima, T., Lavenu, F., Jankowiak, I., and Smirnov, A.: AERONET – A federated instrument network and data archive for aerosol characterization, Remote Sens. Environ., 66, 1–16, doi:10.1016/S0034-4257(98)00031-5, 1998.

IPCC (Intergovernmental Panel on Climate Change): Climate Change 2013: The Physical Science Basis. Contribution of Working Group I to the Fifth Assessment Report of the Intergovernmental Panel on Climate Change, Cambridge University Press, Cambridge, UK and New York, NY, USA, 1535 pp., 2013.

Kappos, A. D., Bruckmann, P., Eikmann, T., Englert, N., Heinrich, U., Hoppe, P., Koch, E., Krause, G. H. M., Kreyling, W. G., Rauchfuss, K., Rombout, P., Schulz-Klemp, V., Thiel, W. R., and Wichmann, H. E.: Health effects of particles in ambient air, Int. J. Hyg. Environ. Health, 207, 399–407, doi:10.1078/1438-4639-00306, 2004.

Kaufman, Y. J., Tanré, D., and Boucher, O.: A satellite view of aerosols in the climate system, Nature, 419, 215–223, 2002.

Kim, J., Lee, J., Lee, H. C., Higurashi, A., Takemura, T., and Song, C. H.: Consistency of the aerosol type classification from satellite remote sensing during the Atmospheric Brown Cloud–East Asia Regional Experiment campaign, J. Geophys. Res.-Atmos., 112, D22S33, doi:10.1029/2006JD008201, 2007.

Kim, S.-W., Yoon, S.-C., Kim, J., and Kim, S.-Y.: Seasonal and monthly variations of columnar aerosol optical properties over east Asia determined from multi-year MODIS, LIDAR, and AERONET Sun/sky radiometer measurements, Atmos. Environ., 41, 1634–1651, doi:10.1016/j.atmosenv.2006.10.044, 2007.

Koelemeijer, R. B. A., Homan, C. D., and Matthijsen, J.: Comparison of spatial and temporal variations of aerosol optical thickness and particulate matter over Europe, Atmos. Environ., 40, 5304–5315, doi:10.1016/j.atmosenv.2006.04.044, 2006.

Kumar, N., Chu, A., and Foster, A.: An empirical relationship between $PM_{2.5}$ and aerosol optical depth in Delhi Metropolitan, Atmos. Environ., 41, 4492–4503, 2007.

Lee, J., Kim, J., Song, C. H., Kim, S. B., Chun, Y., Sohn, B. J., and Holben, B. N.: Characteristics of aerosol types from AERONET sunphotometer measurements, Atmos. Environ., 44, 3110–3117, doi:10.1016/j.atmosenv.2010.05.035, 2010.

Levy, R. C., Remer, L. A., Mattoo, S., Vermote, E. F., and Kaufman, Y. J.: Second-generation operational algorithm: Retrieval of aerosol properties over land from inversion of Moderate Resolution Imaging Spectroradiometer spectral reflectance, J. Geophys. Res.-Atmos., 112, D13211, doi:10.1029/2006jd007811, 2007.

Levy, R. C., Mattoo, S., Munchak, L. A., Remer, L. A., Sayer, A. M., Patadia, F., and Hsu, N. C.: The Collection 6 MODIS aerosol products over land and ocean, Atmos. Meas. Tech., 6, 2989–3034, doi:10.5194/amt-6-2989-2013, 2013.

Liu, Y., Park, R. J., Jacob, D. J., Li, Q. B., Kilaru, V., and Sarnat, J. A.: Mapping annual mean ground-level $PM_{2.5}$ concentrations using Multiangle Imaging Spectroradiometer aerosol optical thickness over the contiguous United States, J. Geophys. Res.-Atmos., 109, D22206, doi:10.1029/2004jd005025, 2004.

Liu, Y., Sarnat, J. A., Kilaru, V., Jacob, D. J., and Koutrakis, P.: Estimating ground-level $PM_{2.5}$ in the eastern United States using satellite remote sensing, Environ. Sci. Technol., 39, 3269–3278, 2005.

Liu, Y., Franklin, M., Kahn, R., and Koutrakis, P.: Using aerosol optical thickness to predict ground-level $PM_{2.5}$ concentrations in the St. Louis area: A comparison between MISR and MODIS, Remote Sens. Environ., 107, 33–44, doi:10.1016/j.rse.2006.05.022, 2007.

Munchak, L. A., Levy, R. C., Mattoo, S., Remer, L. A., Holben, B. N., Schafer, J. S., Hostetler, C. A., and Ferrare, R. A.: MODIS 3 km aerosol product: applications over land in an urban/suburban region, Atmos. Meas. Tech., 6, 1747–1759, doi:10.5194/amt-6-1747-2013, 2013.

Murayama, T., Sugimoto, N., Uno, I., Kinoshita, K., Aoki, K., Hagiwara, N., Liu, Z. Y., Matsui, I., Sakai, T., Shibata, T., Arao, K., Sohn, B. J., Won, J. G., Yoon, S. C., Li, T., Zhou, J., Hu, H. L., Abo, M., Iokibe, K., Koga, R., and Iwasaka, Y.: Ground-based network observation of Asian dust events of April 1998 in east Asia, J. Geophys. Res.-Atmos., 106, 18345–18359, 2001.

Ogunjobi, K. O., Kim, Y. J., and He, Z.: Influence of the total atmospheric optical depth and cloud cover on solar irradiance components, Atmos. Res., 70, 209–227, doi:10.1016/j.atmosres.2004.01.003, 2004.

Pan, X. L., Yan, P., Tang, J., Ma, J. Z., Wang, Z. F., Gbaguidi, A., and Sun, Y. L.: Observational study of influence of aerosol hygroscopic growth on scattering coefficient over rural area near Beijing mega-city, Atmos. Chem. Phys., 9, 7519–7530, doi:10.5194/acp-9-7519-2009, 2009.

Pelletier, B., Santer, R., and Vidot, J.: Retrieving of particulate matter from optical measurements: A semiparametric approach, J. Geophys. Res.-Atmos., 112, D06208, doi:10.1029/2005JD006737, 2007.

Pope, C. A., Burnett, R. T., Thun, M. J., Calle, E. E., Krewski, D., Ito, K., and Thurston, G. D.: Lung cancer, cardiopulmonary mortality, and long-term exposure to fine particulate air pollution, J. Am. Med. Assoc., 287, 1132–1141, 2002.

Remer, L. A., Kaufman, Y. J., Tanre, D., Mattoo, S., Chu, D. A., Martins, J. V., Li, R. R., Ichoku, C., Levy, R. C., Kleidman, R. G., Eck, T. F., Vermote, E., and Holben, B. N.: The MODIS aerosol algorithm, products, and validation, J. Atmos. Sci., 62, 947–973, 2005.

Schaap, M., Apituley, A., Timmermans, R. M. A., Koelemeijer, R. B. A., and de Leeuw, G.: Exploring the relation between aerosol optical depth and $PM_{2.5}$ at Cabauw, the Netherlands, Atmos. Chem. Phys., 9, 909–925, doi:10.5194/acp-9-909-2009, 2009.

Schuster, G. L., Dubovik, O., and Holben, B. N.: Angstrom exponent and bimodal aerosol size distributions, J. Geophys. Res., 111, D07207, doi:10.1029/2005JD006328, 2006.

Song, C.-K., Ho, C.-H., Park, R. J., Choi, Y.-S., Kim, J., Gong, D.-Y., and Lee, Y.-B.: Spatial and seasonal variations of surface PM_{10} concentration and MODIS aerosol optical depth over China, Asia. Pac. J. Atmos. Sci., 45, 33–43, 2009.

van Donkelaar, A., Martin, R. V., Brauer, M., Kahn, R., Levy, R., Verduzco, C., and Villeneuve, P. J.: Global estimates of ambient fine particulate matter concentrations from satellite-based aerosol optical depth: development and application, Environ. Health. Persp., 118, 847–855, doi:10.1289/ehp.0901623, 2010.

Wang, J. and Christopher, S. A.: Intercomparison between satellite-derived aerosol optical thickness and $PM_{2.5}$ mass: Implications for air quality studies, Geophys. Res. Lett., 30, 2095, doi:10.1029/2003gl018174, 2003.

Wang, Z. F., Chen, L. F., Tao, J. H., Zhang, Y., and Su, L.: Satellite-based estimation of regional particulate matter (PM) in Beijing using vertical-and-RH correcting method, Remote Sens. Environ., 114, 50–63, doi:10.1016/j.rse.2009.08.009, 2010.

WHO (World Health Organization): WHO Air quality guidelines for particulate matter, ozone, nitrogen dioxide and sulfur dioxide – global update 2005, WHO Press, World Health Organization, Geneva, Switzerland, 20 pp., 2005.